

Resonant terahertz transmissions through metal hole array on silicon substrate

Xiao Xiao¹, Wu Jinbo¹, Yuki Sasagawa², Fumiaki Miyamaru^{2,4}, Mengying Zhang¹, Mitsuo W. Takeda², Chunyin Qiu³, Weijia Wen^{1,*} and Ping Sheng¹

¹*Department of Physics, Hong Kong University of Science and Technology, Clear Water Bay, Kowloon, Hong Kong, China*

²*Department of Physics, Faculty of Science, Shinshu University, Matsumoto 390-8621, Japan*

³*Key Lab of Acoustic and Photonic Materials and Devices of Ministry of Education and Department of Physics, Wuhan University, Wuhan 430072, China*

⁴*PRESTO, Japan Science and Technology Agency, Aoba, Sendai 980-8577, Japan.*

*phwen@ust.hk

Abstract: We have observed resonant terahertz transmission peaks in samples comprising perforated periodic hole array in a metal film, covered with a high dielectric substrate. These resonant transmissions arise from the interplay between waveguide modes in dielectric substrate and the periodic hole array in the metal film. Finite difference time domain (FDTD) simulations show good agreement with the data, in support of the proposed mechanism. Inducing additional resonant transmissions using guided modes can lead to the ease in tuning the transmission peak frequencies that are potentially useful to terahertz (THz) bio-sensing.

©2010 Optical Society of America

OCIS codes: (120.7000) Transmission; (260.5740) Resonance; (050.2770) Gratings.

References and links

1. T. W. Ebbesen, H. J. Lezec, H. F. Ghaemi, T. Thio, and P. A. Wolff, "Extraordinary optical transmission through sub-wavelength hole arrays," *Nature* **391**(6668), 667–669 (1998).
2. F. J. García de Abajo, "Colloquium: Light scattering by particle and hole arrays," *Rev. Mod. Phys.* **79**(4), 1267–1290 (2007).
3. M. Liscidini, and J. E. Sipe, "Enhancement of diffraction for biosensing applications via Bloch surface waves," *Appl. Phys. Lett.* **91**(25), 253125 (2007).
4. F. Miyamaru, M. W. Takeda, T. Suzuki, and C. Otani, "Highly sensitive surface plasmon terahertz imaging with planar plasmonic crystals," *Opt. Express* **15**(22), 14804–14809 (2007).
5. Z. Ruan, and M. Qiu, "Enhanced transmission through periodic arrays of subwavelength holes: the role of localized waveguide resonances," *Phys. Rev. Lett.* **96**(23), 233901 (2006).
6. W. Zhang, A. K. Azad, J. Han, J. Xu, J. Chen, and X. C. Zhang, "Direct observation of a transition of a surface plasmon resonance from a photonic crystal effect," *Phys. Rev. Lett.* **98**(18), 183901 (2007).
7. F. J. Garcia-Vidal, L. Martin-Moreno, H. J. Lezec, and T. W. Ebbesen, "Focusing light with a single subwavelength aperture flanked by surface corrugations," *Appl. Phys. Lett.* **83**, 4500 (2003).
8. H. J. Lezec, A. Degiron, E. Devaux, R. A. Linke, L. Martin-Moreno, F. J. Garcia-Vidal, and T. W. Ebbesen, "Beaming light from a subwavelength aperture," *Science* **297**(5582), 820–822 (2002).
9. D. Qu, and D. Grischkowsky, "Observation of a new type of THz resonance of surface plasmons propagating on metal-film hole arrays," *Phys. Rev. Lett.* **93**(19), 196804 (2004).
10. F. Miyamaru, Y. Sasagawa, and M. W. Takeda, "Effect of dielectric thin films on reflection properties of metal hole arrays," *Appl. Phys. Lett.* **96**(2), 021106 (2010).
11. S. A. Kuznetsov, M. Navarro-Cía, V. V. Kubarev, A. V. Gelfand, M. Beruete, I. Campillo, and M. Sorolla, "Regular and anomalous extraordinary optical transmission at the THz-gap," *Opt. Express* **17**(14), 11730–11738 (2009).
12. R. Ortuño, C. García-Meca, F. J. Rodríguez-Fortuño, J. Martí, and A. Martínez, "Multiple extraordinary optical transmission peaks from evanescent coupling in perforated metal plates surrounded by dielectrics," *Opt. Express* **18**(8), 7893–7898 (2010).
13. J. Han, A. Lakhtakia, Z. Tian, X. Lu, and W. Zhang, "Magnetic and magnetothermal tunabilities of subwavelength-hole arrays in a semiconductor sheet," *Opt. Lett.* **34**(9), 1465–1467 (2009).
14. J. Han, X. Lu, and W. Zhang, "Terahertz transmission in subwavelength holes of asymmetric metal-dielectric interfaces: The effect of a dielectric layer," *J. Appl. Phys.* **103**(3), 033108 (2008).

15. A. Yu. Nikitin, F. J. García-Vidal, and L. Martín-Moreno, "Enhanced optical transmission, beaming and focusing through a subwavelength slit under excitation of dielectric waveguide modes," *J. Opt. A* **11**, 125702 (2009).
 16. Simulations were performed using the software CONCERTO 6.5, Vector Fields Limited, England, 2007.
 17. V. Lomakin, and E. Michielssen, "Enhanced transmission through metallic plates perforated by arrays of subwavelength holes and sandwiched between dielectric slabs," *Phys. Rev. B* **71**(23), 235117 (2005).
 18. See for example: K. Q. Zhang, and D. Li, "*Electromagnetic theory for Microwaves and Optoelectronics*" (2nd Edition, Springer, Berlin, 2008).
-

1. Introduction

Extraordinary transmission (ET) through a periodically perforated metal plate may be attributed to the electromagnetic (EM) grating resonances that can occur at frequencies where the structure dimensions properly match the relevant wavelength [1]. Much attention has been focused on this phenomenon recently, owing to its potential applications in various areas [2–9]. In particular, one of the most important characteristics of ET is the significant increase in the near-field intensity of the transmitted radiation, making them useful for the detection of small amounts of sample [10]. However, for such applications tuning the resonant frequencies can be very important, and it would be desirable to have additional transmission frequencies in the THz regime in addition to the usual cases.

In this paper, we report an advance along this direction. By introducing an overlayer of relatively thick dielectric material [11–15] with high refractive index on the perforated metal layer, the extra resonant transmission peaks were found to appear at frequencies of the guided modes in the overlayer. The observations and the proposed mechanism of induced transmission via guided modes are supported by good agreement between theory and experiment. In what follows, we explore the relationship between the dispersion relations of the waveguide modes in the dielectric layer and show how they can couple to the perforated hole array in the metal film. A simple equation for determining the resonant frequencies is obtained, from which one can predict the resonant transmission frequencies from the characteristics of the dielectric layer. Simulation of the electric field at various resonant frequencies is shown to yield excellent support to the waveguide-mode mechanism. We also study the dependence of transmission peak frequencies on the thicknesses of substrate. The experimental measurements show good agreement with the theoretical calculations. This characteristic provides a method of tuning the resonant transmission peaks.

2. Sample fabrication, experimental measurements and simulation

An image of the sample studied in the experiment is shown in Fig. 1(a). Holes 160 μm in diameter (corresponding to a cutoff frequency of 1.1 THz) were perforated in a 3 μm -thick copper film, with a simple square lattice structure and a lattice constant of 300 μm . The dielectric layer is an intrinsic silicon film that is 500 μm in thickness. Configuration of the sample is shown in Figs. 1(b) and 1(c). In Fig. 1(c) we also define the coordinate system related to our sample geometry. The copper layer together with a 100nm adhesion layer of Ti/W was first sputtered on a 500 μm thick silicon substrate, and then photo resist was patterned by standard photolithography before copper and Ti/W were etched by hydrogen peroxide in room temperature and 60 °C, respectively. The Fabry-Perot transmission spectrum of the pure silicon layer is shown in the inset of Fig. 1(d), from which the dielectric constant of the silicon layer is determined to be 12.

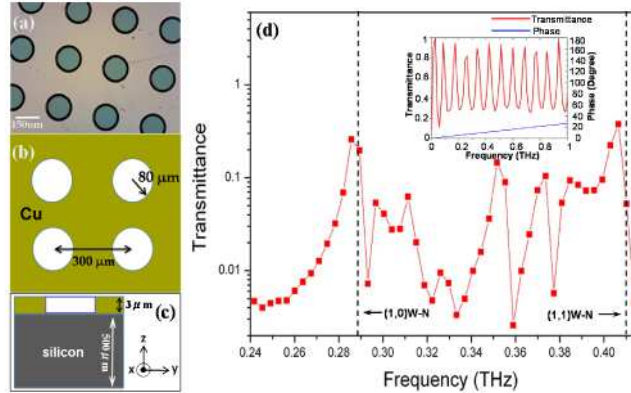


Fig. 1. (a) A microscopic optical image of the sample. (b) Top view of the sample, showing the hole array in the Cu metallic film. (c) Side view of the sample together with the coordinate system defined relative to the sample geometry, showing the thick silicon overlayer (bottom) bonded to the metallic layer with the hole array. (d) The transmission spectrum of the sample. The Wood's anomaly (W-N) frequencies are delineated by the black dashed lines, denoted by the (1,0) and (1,1) gratings of the square lattice. The extra transmission peaks are associated with the guided modes in the silicon overlayer. Inset: Fabry-Perot transmission characteristic of the silicon substrate. From the interference pattern a dielectric constant of 12 is deduced.

We measured the transmission spectrum of the sample by using the THz time domain spectroscopy (THz-TDS). The terahertz wave pulses were emitted from a dipole-type photoconductive antenna illuminated by a 117-fs laser pumping pulses at 800 nm. The detection was achieved by a dipole-type photoconductive antenna gated with time-delayed probing laser pulses that were diverted from the pumping pulses. By varying the difference between the optical path lengths of the pumping and probing pulses, the waveform of the terahertz wave was measured in the time domain. The Fourier-transformed transmission spectrum in frequency domain is shown in Fig. 1(d). It is seen that there are more resonant peaks than what are usually expected around Wood's anomaly frequencies (denoted by the two black dashed lines).

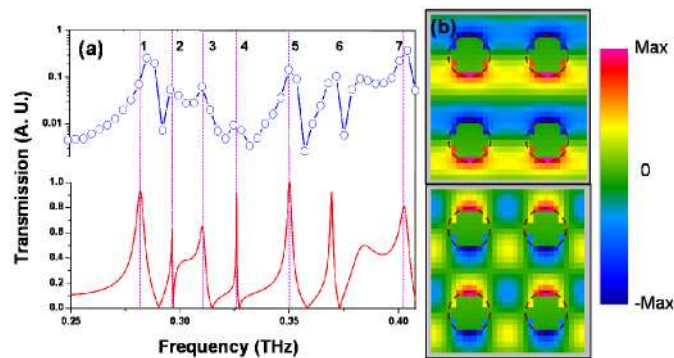


Fig. 2. (a) Upper panel: the measured transmission spectrum. Lower panel: FDTD simulated transmission spectrum. Clear correspondence is seen. (b) Distribution of the E_z component on the x - y interfacial plane between the metal film and the dielectric substrate at resonant transmission frequencies. The positions of the holes in the metal film are delineated by the dashed lines. The upper panel is for the field distributions at the first 6 resonant frequencies, which have the same pattern except for the differences in magnitudes; the lower panel is for the field distribution at the 7th resonant frequency. The waveguiding mode characters are clearly seen from the patterns shown.

In order to understand the experimental results, the transmission spectrum is simulated by using the FDTD approach [16]. In the simulation a 2×2 superlattice of the sample was

placed in a box with the periodic boundary condition and the incident plane wave was launched normal to the surface of the sample. A 500 μm thick dielectric layer with a dielectric constant 12 was used in the simulations, and the metal layer has a thickness of 3 μm . Perfect conductor boundary condition was used for the perforated metal film. The simulated results are shown in the lower panel of Fig. 2(a). Good agreement with the experiment is clearly seen. Except for the peaks labeled by 1 (0.282THz) and 7 (0.402THz) around the Wood's anomaly frequencies, five other peaks are also visible, labeled by 2, 3, 4, 5 and 6 with frequencies respectively located at 0.296THz, 0.311THz, 0.326THz, 0.351THz, 0.369THz. Moreover, the field distributions of the z-component electric field on the interface between metal and dielectric at these resonant frequencies are shown in Fig. 2(b). The field patterns for the peaks of 1-6, corresponding to the (1, 0) diffraction mode, are exactly the same except the differences in their magnitudes. This is shown in the upper panel of Fig. 2(b). The field pattern of peak 7, which corresponds to the (1, 1) diffraction mode, is shown in the lower panel of Fig. 2 (b).

3. Analysis and discussion

The ET from the hole array on metal plate can be understood as arising from the interplay between the Bragg surface modes generated by the periodicity and the hole excitations that enhance the field intensity inside the holes. These ET modes generally appear at frequencies close to that of the Wood's anomaly and the attendant Bragg surface wave is bound close to the metal surface [17]. In our case, the silicon layer supports guided modes with low loss propagation parallel to the metal surface. These tangential propagating waveguide modes are built up by the scattering of the metal hole array, and these guided modes can also interact with the hole array that serves as one bounding surface of the waveguide, hence leading to extraordinary transmissions. However, if the dielectric layer is thick enough, there can be many guided modes, leading to the many extra ET modes.

To give a more concrete and clearer picture, we analyze the dispersion of the waveguide mode bound in the silicon layer. For simplicity, we neglect the effect of holes (due to their subwavelength characteristics) in obtaining the dispersion relation and the guided mode configuration. The coupling to the hole gratings will be treated separately on the basis of the guided modes and their dispersion relations thus obtained. The effect of the coupling will be shown to manifest itself as zone folding as well as the intersection of the folded dispersion with the light line in air, leading to transmission. Since our waveguide is asymmetric in the sense that one bounding surface is the dielectric-air interface whereas the other bounding surface is the dielectric-metal interface, we shall treat the metal as a "mirror" reflecting surface (allowing only normal electric component and tangential magnetic component) so that the analysis can be simplified to that of a dielectric waveguide with twice the original thickness in air [18]. However, because of the boundary condition requirement, only the even TM modes in the symmetric waveguide can contribute. Their dispersion relations are given by the equation:

$$\sqrt{k_t^2 - \frac{\omega^2}{c_a^2}} = \frac{\varepsilon_a}{\varepsilon_{si}} \sqrt{\frac{\omega^2}{c_{si}^2} - k_t^2} \tan \left(2 \sqrt{\frac{\omega^2}{c_{si}^2} - k_t^2} h - m\pi \right), m = 1, 2, \dots \quad (1)$$

where k_t is a wave vector parallel to the interface between metal and dielectric, $\varepsilon_a = 1$ is the dielectric constant of air, $\varepsilon_{si} = 12$ is the dielectric constant of silicon, c_{si} is the light velocity in silicon, c_a is the light velocity in air, ω is the angular frequency, and h denotes the silicon layer thickness.

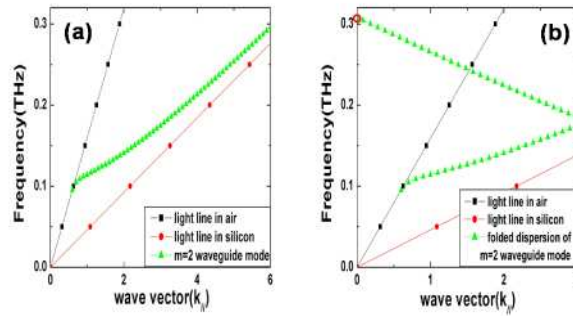


Fig. 3. (a) Dispersion relation for the $m = 2$ waveguide mode in dielectric layer plotted together with both the light lines in air (for $\theta = 90^\circ$ mode) and in silicon. Here θ is the angle between the incident wave vector and the z axis. (b) Folded dispersion of the waveguide mode (and light lines for $\theta = 90^\circ$ mode) in the first BZ; the red circle denotes the intersection of the dispersion of the guided mode and the normally propagating light line ($k_{||} = 0$), implies a normally propagating transmission peak. From this analysis, the equation determining the frequencies of the resonant transmissions with (0, 1) surface diffraction mode must satisfy the following condition:

In order to illustrate our result, the second mode ($m = 2$) together with light lines in air and silicon (representing modes propagating parallel to the interface) are plotted in Fig. 3(a). The effect of periodicity is accounted for by zone folding at the edge of the first BZ (Fig. 3 (b)). The folded dispersion curve is seen to intersect the light line in air. The red circle, which denotes the intersection between folded dispersion curve and normally propagating light line ($k_{||} = 0$), implies a normally propagating transmission peak. From this analysis, the equation determining the frequencies of the resonant transmissions with (0, 1) surface diffraction mode must satisfy the following condition:

$$\left(\frac{2\pi}{d}\right)^2 + \left(\frac{m\pi}{2h}\right)^2 = \varepsilon_{si} \frac{\omega^2}{c^2}, m = 1, 2, \dots \quad (2)$$

where d is the lattice constant and h is the thickness of the silicon layer. From this equation, we determine that there are 6 resonant peaks. The first peak, which was thought to be the first Wood's anomaly, in fact results from the $m = 1$ TM waveguide mode and its position is predicted to be 0.292 THz. The other five peaks are predicted to be 0.302THz, 0.317THz, 0.337THz, 0.361THz and 0.388THz. These predictions agree very well with the observations as seen in Fig. 2. The slight shifts between the theory and experimental frequencies may result from the fact we did not consider the effect of the hole size and the thickness of the metal layer. However, there is no doubt that the simple model captures the essential physics extremely well. Except the main contribution of waveguide modes to the resonant transmission, Fabry-Perot (F-P) mode may also play some role. In our study frequency region, there are two F-P modes locating at 0.2601THz and 0.3468THz. The effects of F-P modes to transmission enhancement may be observed from the fact that the transmission peaks around them are broadened.

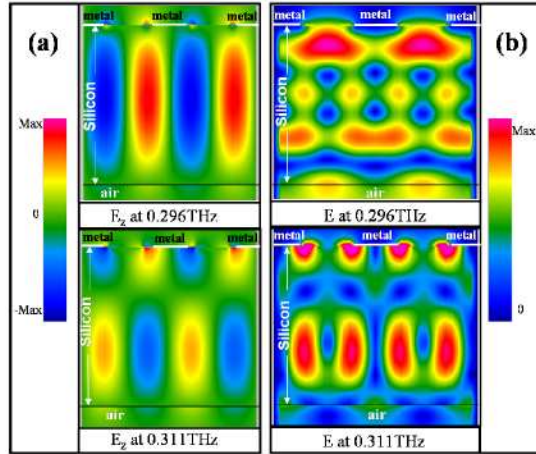


Fig. 4. (a) Simulated field distributions of the E_z component of the electric field at resonant frequencies 0.296 THz and 0.311 THz on the x - z plane passing through two origins of circular holes. (b) Simulated total electric field on the same x - z plane. Concentration of the field intensity in the vicinity of the holes is clearly seen.

We have carried out FDTD simulations on the z component of the electric field as well as the total electric field distribution, so as to focus on the coupling between the waveguide modes in the silicon layer and the hole array. We chose the x - z plane (perpendicular to the interface) passing through the origins of two circular holes as the simulation plane. The simulation results at two resonant frequencies (noted in the figure) are shown in Fig. 4. The distributions of the z component of electric field at these two resonant frequencies are shown in Fig. 4(a). The waveguide mode configurations in the silicon layer are clearly seen, i.e., the distribution pattern of E_z at 0.296THz exactly corresponds to the $m = 2$ waveguide mode, and the field pattern at 0.311THz corresponds to the $m = 3$ waveguide mode. The coupling of the waveguide modes with metal hole array is seen as the field modification around the holes that causes the total electric field around the holes to be much stronger (Fig. 4 (b)), leading resonant transmission.

4. Substrate thickness effect

One of the advantages of ET modified by waveguide modes is that the frequency of resonant transmission peaks can be changed by the thickness of substrates (See Eq. (2)). To verify it, we have fabricated the samples with different thicknesses by etching the silicon substrates. Figure 5 (a) shows the transmission spectra of metal hole arrays with four substrate thicknesses. We find that the resonant transmission peaks shift to lower frequency as the thickness of the substrate increases. To give a quantitative analysis, we calculated the dependence of the transmission peak frequency for different waveguide modes. The calculated relations between thicknesses and positions of transmission peaks for different waveguide modes are shown in Fig. 5 (b). The measured transmission peaks are also shown as square dots in Fig. 5 (b). One can find that the experimental data agree well with the calculated line for low index modes ($m = 1$ and $m = 2$). On the other hand, the derivation between experiment and theory becomes slightly larger for higher index modes ($m = 3$, $m = 4$ and $m = 5$). This is attributed to the fact that we neglected the size of the hole and the thickness of metal layer in our calculation.

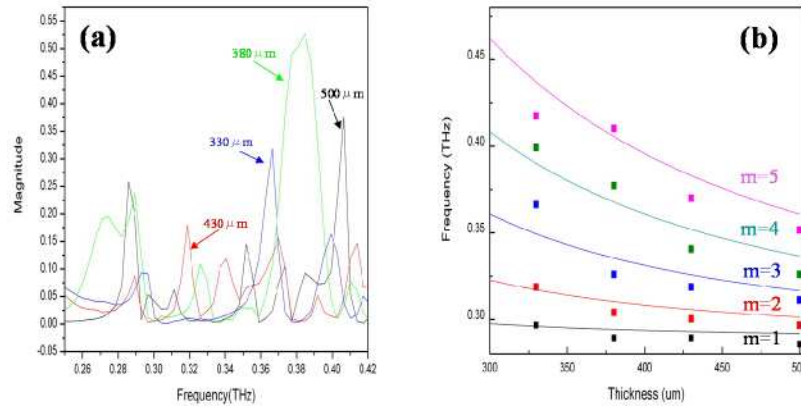


Fig. 5. (a) The transmission spectra of samples with different substrate thicknesses (Red line: 430 μm , blue line: 330 μm , green line: 380 μm and black line: 500 μm). (b) The relation between thickness and peak frequency for different modes: solid lines and square dots are calculated and measured transmission peaks for different substrate thicknesses, respectively. For these modes, black color line and square dots are for $m = 1$ mode, red color line and dots are for $m = 2$ mode, blue color line and dots are for $m = 3$ mode, olive color line and dots are for $m = 4$ mode, and pink color line and dots are for $m = 5$ modes.

5. Conclusion

We have observed resonant transmissions in the sub-THz region, induced by guided modes in the dielectric (silicon) substrate. Theoretical analysis of guided modes as well as the FDTD simulations gives support to this mechanism. The extra resonant transmissions may be useful in THz sensing by offering easier tuning of the ET frequencies to the desired detection frequencies.

Acknowledgments

Financial support from Hong Kong RGC grants 603207, N_HKUST632/07 and HKUST3/06C is hereby gratefully acknowledged.